

RESOLUTION ASSESSMENT IN DYNAMIC IMAGE FORMATION

Mark D. Butala*

Jet Propulsion Laboratory, California Institute of Technology
National Aeronautics and Space Administration

ABSTRACT

Remote sensing and astronomical image formation is often complicated by deficiencies in measurement quality, density, or diversity. Penalized likelihood methods can incorporate additional first-principles physical prior knowledge and improve the image reconstructions, but a systematic bias is unavoidable as a consequence. This work derives theory to understand the bias and develops a computational tool to probe its effect on the reconstructed image and bound resolution limits. Though the focus is on image formation, the contributions of this paper apply to any inference problem that can be expressed under the linear state-space signal model.

Index Terms— remote sensing; multidimensional signal processing; recursive estimation; Kalman filter

1. INTRODUCTION

Inverse problems involving line integral or tomographic projection measurements are common in remote sensing and astronomy, with applications ranging from radio interferometry to solar tomography [1]. Many inversion methods exist to solve these problems but each makes certain *a priori* assumptions to trade-off a bias in the solution for increased stability [1]. This work derives a method to quantify the trade-off's impact on achievable resolution for a large class of image formation problems solved with penalized likelihood methods.

Although resolution bounds exist for dynamic medical tomography [2], this work addresses a more general class of non-stationary linear inverse problems. When compared to similar problems in remote sensing and astronomy, medical imaging has, in general, the benefit of relatively high SNR and densely sampled projection observations. Another general difference is that astronomical image formation can require extremely long observing intervals when, for example, the Earth's rotation is utilized in radio interferometry or revolution about the Sun in solar tomography [1], [3]. Stationarity is an increasingly good assumption as the observation interval shortens but a dynamic solution is often required as the observation interval lengthens.

The theoretical contribution of this paper consists of a time-dependent generalization of Fessler's local impulse response [4]. Though Fessler's latest work [5] also extends the local impulse response to dynamic problems, this effort considers the more general fully stochastic state-space signal model which is amenable to a broad class of data assimilation problems [1]. The local impulse response quantifies the average effect a spatially localized perturbation has on the reconstructed image [4]. Our generalization provides the means to quantify the effect of a localized spatial-temporal perturbation and the extent of the effect defines the average resolution limits, both spatially and temporally. Furthermore, our methodology applies to all problems encountered in state estimation: filtering, prediction, and smoothing [6].

Because the analysis is based on the Kalman filter [6], the theoretical contribution provides a practical tool to compute the dynamic local impulse response and investigate resolution bounds. The spatial and temporal extent of the dynamic local impulse response, often quantified by the full width at half maximum [4], bounds the smallest discernible reconstructed features at one particular spatial-temporal coordinate. Probing these bounds reveals the reconstructed image regions that are least prone to systematic artifacts and can ultimately strengthen the inferred scientific conclusions.

The remainder of the paper is organized in the following manner. Sec. 2 defines the linear static and dynamic signal models. The static impulse response [4] is briefly summarized in Sec. 3. Next, Sec. 4 derives the dynamic impulse response. Sec. 5 details a dynamic tomography example and demonstrates the use of the Kalman filter to compute the local impulse response. Conclusion are given in Sec. 6.

2. SIGNAL MODELS

The linear dynamic signal model is defined by the state-space equations:

$$\mathbf{x}_{i+1} = \mathbf{F}_i \mathbf{x}_i + \mathbf{u}_i \quad (1)$$

$$\mathbf{y}_i = \mathbf{H}_i \mathbf{x}_i + \mathbf{v}_i. \quad (2)$$

In the above, the N -dimensional vector \mathbf{x}_i is the unknown at time index i , the time index has the range $1 \leq i \leq I$, the M -dimensional vector \mathbf{y}_i is the i th measurement, the matrices \mathbf{F}_i

*The author performed the work while completing his dissertation at the University of Illinois at Urbana-Champaign.

and \mathbf{H}_i are known, and the random vectors \mathbf{u}_i and \mathbf{v}_i model uncertainty in the state-transition (1) and forward (2) models. Also, the covariances $\mathbf{Q}_i \triangleq \text{Cov}(\mathbf{u}_i)$, $\mathbf{R}_i \triangleq \text{Cov}(\mathbf{v}_i)$, and $\mathbf{\Pi}_1 \triangleq \text{Cov}(\mathbf{x}_1)$ are known as is the initial state mean $\boldsymbol{\mu}_1 \triangleq E[\mathbf{x}_1]$. We emphasize that [5] considers a similar signal model, but with no uncertainty in the state transition, i.e., $\mathbf{u}_i = \mathbf{0}$.

The linear static signal model assumes $\mathbf{x} = \mathbf{x}_i$ and is obtained when $\mathbf{F}_i = \mathbf{I}$, where \mathbf{I} is the identity matrix, and $\mathbf{u}_i = \mathbf{0}$ in (1). The signal model reduces to

$$\begin{bmatrix} \mathbf{y}_1 \\ \vdots \\ \mathbf{y}_I \end{bmatrix} = \begin{bmatrix} \mathbf{H}_1 \\ \vdots \\ \mathbf{H}_I \end{bmatrix} \mathbf{x} + \begin{bmatrix} \mathbf{v}_1 \\ \vdots \\ \mathbf{v}_I \end{bmatrix} \quad (3)$$

which we will represent by the notation

$$\mathbf{y}_{1:I} = \mathbf{H}_{1:I} \mathbf{x} + \mathbf{v}_{1:I}, \quad (4)$$

the measurement and initial state covariances by $\mathbf{R}_{1:I} \triangleq \text{Cov}(\mathbf{v}_{1:I})$ and $\mathbf{\Pi} \triangleq \text{Cov}(\mathbf{x})$, and the initial state mean by $\boldsymbol{\mu} \triangleq E[\mathbf{x}]$.

3. STATIC IMPULSE RESPONSE

The static local impulse response [4] is defined by

$$\mathbf{l}^j \triangleq \frac{\partial}{\partial [\mathbf{x}]_j} E[\widehat{\mathbf{x}}|\mathbf{x}] \quad (5)$$

where $[\cdot]_j$ denotes the j th component of its vector argument and $\widehat{\mathbf{x}}$ is the estimate of the unknown. For this work, we consider the linear minimum mean square error (LMMSE) estimator given by [6]

$$\widehat{\mathbf{x}} = \boldsymbol{\mu} + (\mathbf{\Pi}^{-1} + \mathbf{H}_{1:I}^T \mathbf{R}_{1:I}^{-1} \mathbf{H}_{1:I})^{-1} \mathbf{H}_{1:I}^T \mathbf{R}_{1:I}^{-1} \cdot (\mathbf{y}_{1:I} - \mathbf{H}_{1:I} \boldsymbol{\mu}). \quad (6)$$

The static local impulse under the linear static signal model defined in Sec. 2 is summarized by the following theorem.

Theorem 1. *The local impulse response (5) for the j th parameter of the LMMSE estimator (6) is given by*

$$\mathbf{l}^j = (\mathbf{\Pi}^{-1} + \mathbf{H}_{1:I}^T \mathbf{R}_{1:I}^{-1} \mathbf{H}_{1:I})^{-1} \mathbf{H}_{1:I}^T \mathbf{R}_{1:I}^{-1} \mathbf{H}_{1:I} \mathbf{e}^j \quad (7)$$

where

$$[\mathbf{e}^j]_n \triangleq \begin{cases} 1, & j = n \\ 0, & \text{otherwise.} \end{cases} \quad (8)$$

Proof. See Section II in [4]. However, it is straightforward to evaluate (5) for the LMMSE estimator (6). \square

4. DYNAMIC IMPULSE RESPONSE

We define the dynamic local impulse response as

$$\mathbf{l}_{i|i'}^{j,k} \triangleq \frac{\partial}{\partial [\mathbf{x}_k]_j} E[\widehat{\mathbf{x}}_{i|i'}|\mathbf{x}_{1:i}] \quad (9)$$

where $\widehat{\mathbf{x}}_{i|i'}$ \triangleq $\widehat{\mathbf{x}}_{i|1:i'}$ denotes the estimate of the state \mathbf{x}_i given the set of measurements $\{\mathbf{y}_k\}_{k=1}^{i'}$. The filtering ($i' = i$) case is addressed by the following theorem and the smoothing ($i' > i$) and prediction ($i' < i$) cases by the subsequent corollary. As in Sec. 3, we consider the LMMSE estimator. For the linear dynamic signal model, filtered LMMSE estimates are given by the Kalman filter and predicted and smoothed estimates by affine transformations of its output [6].

The dynamic local impulse response for the filtered LMMSE estimator is summarized by the following theorem.

Theorem 2. *Consider the filtered LMMSE estimator under the linear dynamic signal model defined in Sec. 2. The filtered local impulse response for the k th time index and j th parameter is denoted by $\mathbf{l}_{i|i}^{j,k}$ and may be computed by processing the following simulated measurements through the Kalman filter with $\boldsymbol{\mu}_1 = \mathbf{0}$:*

$$\mathbf{y}_{1:i} = \mathbf{H}_{1:i}^B \mathbf{e}_k^j \quad (10)$$

where

$$\mathbf{H}_{1:i}^B \triangleq \text{diag}(\mathbf{H}_1, \dots, \mathbf{H}_i) \quad (11)$$

and $\text{diag}(\cdot)$ denotes the block diagonal matrix with its arguments as the block elements. The unit vector \mathbf{e}_k^j is defined by

$$[\mathbf{e}_k^j]_{(l-1)M+1:lM} \triangleq \begin{cases} \mathbf{e}^j, & l = k \\ \mathbf{0}, & \text{otherwise} \end{cases} \quad (12)$$

and $[\cdot]_{(l-1)M+1:lM}$ selects the l th block of length M from its vector argument.

Proof. First, the Kalman filter is an affine function of the measurements [6], meaning it may be written in the form

$$\widehat{\mathbf{x}}_{i|i} = \mathbf{A}_i \mathbf{y}_{1:i} + \mathbf{b}_i \quad (13)$$

and, because the Kalman filter computes LMMSE estimates, the above parameters are given by [6]

$$\mathbf{A}_i = \text{Cov}(\mathbf{x}_i, \mathbf{y}_{1:i}) \text{Cov}(\mathbf{y}_{1:i}, \mathbf{y}_{1:i})^{-1} \quad (14)$$

$$\mathbf{b}_i = E[\mathbf{x}_i] - \text{Cov}(\mathbf{x}_i, \mathbf{y}_{1:i}) \text{Cov}(\mathbf{y}_{1:i}, \mathbf{y}_{1:i})^{-1} E[\mathbf{y}_{1:i}] \quad (15)$$

where $\mathbf{y}_{1:i} = \mathbf{H}_{1:i}^B \mathbf{x}_{1:i} + \mathbf{v}_{1:i}$ and $[\mathbf{x}_{1:i}]_{(l-1)N+1:lN} = \mathbf{x}_l$. Next, it is straightforward to derive the expectation of the filtered estimate conditioned on the state:

$$E[\widehat{\mathbf{x}}_{i|i}|\mathbf{x}_{1:i}] = \mathbf{A}_i \mathbf{H}_{1:i}^B \mathbf{x}_{1:i} + \mathbf{b}_i. \quad (16)$$

The dynamic local impulse response (9) is then given by

$$\mathbf{l}_{i|i}^{j,k} = \mathbf{A}_i \mathbf{H}_{1:i}^B \mathbf{e}_k^j \quad (17)$$

and note that (17) is equal to (13) if $\mathbf{y}_{1:i} = \mathbf{H}_{1:i}^B \mathbf{e}_l^j$ and $\mathbf{b}_i = \mathbf{0}$. Finally, it is not difficult to show that

$$E[\mathbf{x}_i] = \mathbf{F}_{i-1} \mathbf{F}_{i-2} \cdots \mathbf{F}_1 \boldsymbol{\mu}_1 \quad (18)$$

and

$$E[\mathbf{y}_{1:i}] = \mathbf{H}_{1:i}^B E[\mathbf{x}_{1:i}] \quad (19)$$

which together imply $\mathbf{b}_i = \mathbf{0}$ if $\boldsymbol{\mu}_1 = \mathbf{0}$. \square

The local impulse response for smoothed and predictive LMMSE estimators are addressed by the following corollary.

Corollary 3. *Consider the LMMSE predictor that produces the estimate $\hat{\mathbf{x}}_{i+1|i}$. The predicted local impulse response $\mathbf{l}_{i+1|i}^{j,k}$ is given by*

$$\mathbf{l}_{i+1|i}^{j,k} = \mathbf{F}_i \mathbf{l}_{i|i}^{j,k}. \quad (20)$$

Furthermore, consider the LMMSE fixed-interval smoother [6] that produces the estimates $\hat{\mathbf{x}}_{i|1:I}$. The smoothed local impulse response $\mathbf{l}_{i|1:I}^{j,k}$ can be computed by processing the simulated measurements $\mathbf{y}_{1:I} = \mathbf{H}_{1:I}^B \mathbf{e}_k^j$ with the Kalman smoother [6] with $\boldsymbol{\mu}_1 = \mathbf{0}$.

Proof. First, the LMMSE prediction of the state \mathbf{x}_{i+1} given the measurements $\mathbf{y}_{1:i}$ is $\hat{\mathbf{x}}_{i+1|i} = \mathbf{F}_i \hat{\mathbf{x}}_{i|i}$. Therefore, following the development in the proof to Theorem 2,

$$\mathbf{l}_{i+1|i}^{j,k} = \mathbf{F}_i \mathbf{A}_i \mathbf{H}_{1:i}^B \mathbf{e}_k^j \quad (21)$$

which can be computed by applying the Kalman filter time update [6] to $\mathbf{l}_{i|i}^{j,k}$.

Next, the Kalman smoother is an affine function of the measurements and can be written in the form

$$\hat{\mathbf{x}}_{i|1:I} = \mathbf{A}'_i \mathbf{y}_{1:I} + \mathbf{b}'_i \quad (22)$$

where

$$\mathbf{A}'_i = \text{Cov}(\mathbf{x}_i, \mathbf{y}_{1:I}) \text{Cov}(\mathbf{y}_{1:I}, \mathbf{y}_{1:I})^{-1} \quad (23)$$

$$\mathbf{b}'_i = E[\mathbf{x}_i] - \text{Cov}(\mathbf{x}_i, \mathbf{y}_{1:I}) \text{Cov}(\mathbf{y}_{1:I}, \mathbf{y}_{1:I})^{-1} E[\mathbf{y}_{1:I}]. \quad (24)$$

The remainder of the argument then closely mirrors the proof to Theorem 2. \square

5. NUMERICAL EXAMPLE

In this numerical experiment, the unknown state is a 16×16 and 48 time step spatial-temporal discretization of a diffusive process, meaning

$$\frac{\partial x_t(\mathbf{s})}{\partial t} = k \nabla_s^2 x_t(\mathbf{s}). \quad (25)$$

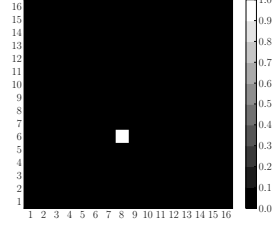


Fig. 1. The unit vector \mathbf{e}_k^j as viewed at time index 29. The unit vector is equal to $\mathbf{0}$ at all other time indices.

Each 40 dB SNR ($\text{SNR} \triangleq 10 \log_{10} \|\mathbf{s}_{1:I}\|_2^2 / \|\mathbf{v}_{1:I}\|_2^2$ where $\mathbf{s}_i \triangleq \mathbf{H}_i \mathbf{x}_i$) measurement consists of $M = 23$ parallel and regularly spaced line integrals of the state that uniformly sweeps through 540° over the 48 time steps. To add a challenge that is often encountered in practice, we model the dynamics as a random walk ($\mathbf{F}_i = \mathbf{I}$) though the diffusive physics governing the experiment are known and linear. We focus on the random walk model because it is often used in practice [1], [3] when the governing physics are complicated and linearized approximations are not useful. The state noise covariance \mathbf{Q}_i is modeled to have 9 bands, indicating each element of \mathbf{u}_i is correlated with immediate neighbors only. The initial state mean is $\boldsymbol{\mu}_1 = \mathbf{0}$ and the initial state covariance is $\boldsymbol{\Pi}_1 = \alpha (\mathbf{D}^T \mathbf{D})$. The parameter α was manually tuned and $\mathbf{D} = [\mathbf{D}_x^T \ \mathbf{D}_y^T]^T$ where \mathbf{D}_x and \mathbf{D}_y are discrete approximations to the spatial derivative in the horizontal and vertical directions.

The ground truth \mathbf{x}_i is shown in the first row of Fig. 2, where each column is a spatial-temporal sample of a simulated diffusion that uses a Dirichlet boundary condition of four hot spots in a cold background at time index $i = 1$. The second and third rows of Fig. 2 show the filtered $\hat{\mathbf{x}}_{i|i}$ and smoothed $\hat{\mathbf{x}}_{i|1:I}$ estimates. As expected and guaranteed in the minimum mean square sense [6], the smoothed estimates are superior to the filtered estimates. Quantitatively, the relative error (e.g., $\|\mathbf{x}_{1:I} - [\hat{\mathbf{x}}_{1|1}^T \cdots \hat{\mathbf{x}}_{I|I}^T]^T\|_2 / \|\mathbf{x}_{1:I}\|_2$) in the filtered case is 0.596 and 0.356 in the smoothed case.

To better understand the resolution implications, we now investigate the local impulse response. We consider the 29th time index and spatial location depicted in Fig. 1. The local impulse responses $\mathbf{l}_{i|i}^{j,29}$ and $\mathbf{l}_{i|1:I}^{j,29}$ are shown in the fourth and fifth rows of Fig. 2. Portions of an impulse response function appearing in gray correspond to absolute values less than one quarter of the impulse response maximum. The filtered local impulse response $\mathbf{l}_{i|i}^{j,29}$ is uniformly equal to 0 at time indices less than $i = 29$. This is expected because the filtered estimates are causal. Also, note that the smoothed local impulse response function decays more quickly in time than in the filtered case. We conclude and could even predict that the relative spatial compactness of the smoothed dynamic local impulse response $\mathbf{l}_{i|1:I}^{j,29}$ away from time index $i = 29$ translates to enhanced reconstruction fidelity at the spatial-temporal coordinate under study.

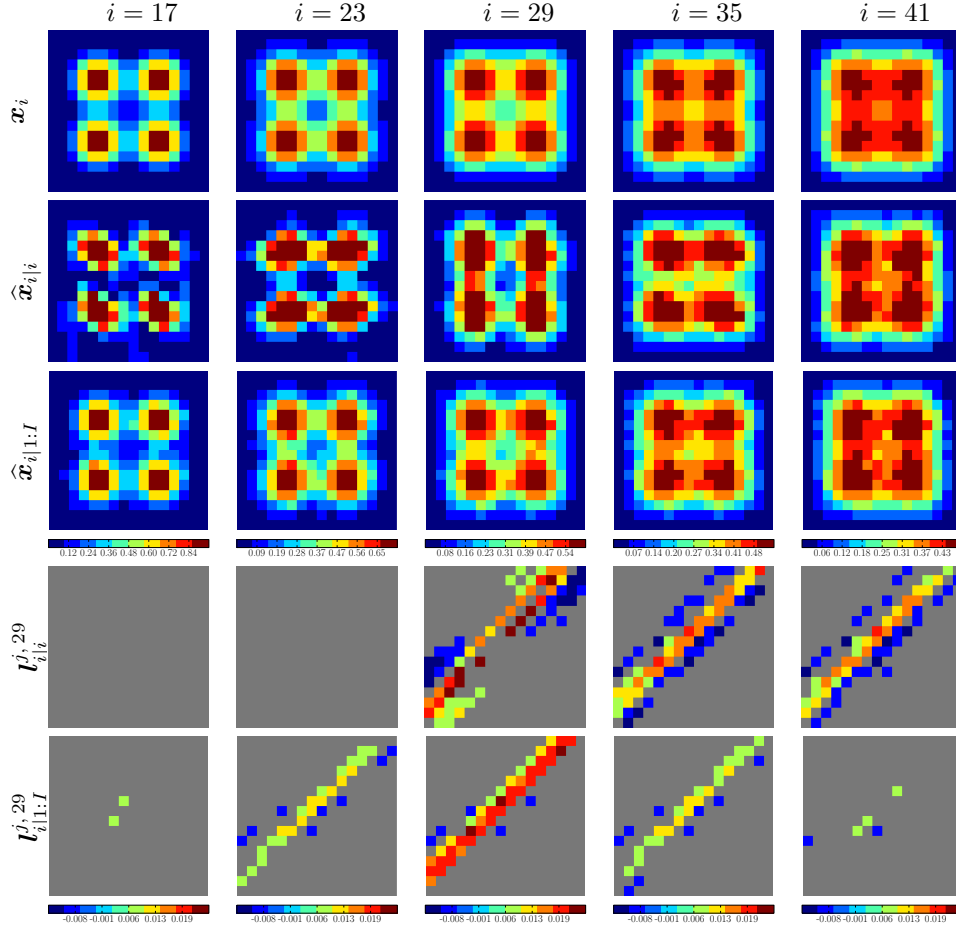


Fig. 2. First row: the experimental ground truth \mathbf{x}_i . Second and third rows: the filtered ($\hat{\mathbf{x}}_{i|i}$) and smoothed ($\hat{\mathbf{x}}_{i|1:I}$) estimates of the ground truth given noisy projective measurements. Fourth and fifth rows: the filtered ($l_{i|k}^{j,k}$) and smoothed ($l_{i|1:I}^{j,k}$) dynamic impulse responses at time index $k = 29$. Note that the first three and the last two rows are each displayed on a common scale.

6. CONCLUSIONS

This paper has addressed the problem of assessing resolution limits in linear dynamic image formation. The numerical experiment demonstrates that smoothing can provide substantial benefits in dynamic tomography. Furthermore, though the focus has been on image formation, the analysis and tools developed in this work apply to a broad class of penalized likelihood methods. Lastly, [4] focuses mainly on the nonlinear case and the results of this work can similarly extend to the analysis of nonlinear dynamic inverse problems.

7. REFERENCES

- [1] M. D. Butala, F. Kamalabadi, R. A. Frazin, and Y. Chen, “Dynamic tomographic imaging of the solar corona,” *IEEE J. Sel. Topics Signal Process.*, vol. 2, pp. 755–766, 2008.
- [2] N. P. Willis and Y. Bresler, “Optimal scan for time varying tomographic imaging I: Theoretical analysis and fundamental limitations,” *IEEE Trans. Image Process.*, vol. 4, no. 5, pp. 642–653, 1995.
- [3] M. D. Butala, R. J. Hewett, R. A. Frazin, and F. Kamalabadi, “Dynamic three-dimensional tomography of the solar corona,” *Solar Phys.*, vol. 262, pp. 495–509, 2010.
- [4] J. A. Fessler and W. L. Rogers, “Spatial resolution properties of penalized-likelihood image reconstruction: Space-invariant tomographs,” *IEEE Trans. Image Process.*, vol. 5, pp. 1346–1358, 1996.
- [5] S. Y. Chun and J. A. Fessler, “Spatial resolution and noise properties of regularized motion-compensated image reconstruction,” in *Proc. IEEE ISBI*, 2009, pp. 863–866.
- [6] T. Kailath, A. H. Sayed, and B. Hassibi, *Linear Estimation*. Upper Saddle River, NJ: Prentice-Hall, 2000.